A generalisation of J2-flow theory for polar continua

Document status and date:
Published: 01/01/1993

Document Version:
Publisher's PDF, also known as Version of Record (includes final page, issue and volume numbers)

Please check the document version of this publication:

• A submitted manuscript is the version of the article upon submission and before peer-review. There can be important differences between the submitted version and the official published version of record. People interested in the research are advised to contact the author for the final version of the publication, or visit the DOI to the publisher's website.
• The final author version and the galley proof are versions of the publication after peer review.
• The final published version features the final layout of the paper including the volume, issue and page numbers.

Link to publication

A generalisation of J_2-flow theory for polar continua

René de Borst

Delft University of Technology, Department of Civil Engineering/TNO Building and Construction Research, P.O. Box 5048, 2600 GA Delft, The Netherlands

A pressure-dependent J_2-flow theory is proposed for use within the framework of the Cosserat continuum. To this end the definition of the second invariant of the deviatoric stresses is generalised to include couple-stresses, and the strain-hardening hypothesis of plasticity is extended to take account of micro-curvatures. The temporal integration of the resulting set of differential equations is achieved using an implicit Euler backward scheme. This return-mapping algorithm results in an exact satisfaction of the yield condition at the end of the loading step. Moreover, the integration scheme is amenable to exact linearisation, so that a quadratic rate of convergence is obtained when Newton's method is used. An important characteristic of the model is the incorporation of an internal length scale. In finite element simulations of localisation, this property warrants convergence of the load–deflection curve to a physically realistic solution upon mesh refinement and to a finite width of the localisation zone. This is demonstrated for an infinitely long shear layer and for a biaxial specimen composed of a strain-softening Drucker–Prager material.

1. Introduction

When testing structures composed of materials such as concrete, rock and soil, a marked peak in the load–displacement curve is often found followed by a descending branch. Depending on the type of material, the residual load-carrying capacity of the structure may only be marginally below the peak strength or may vanish altogether.

The classical approach towards this behaviour is to simply extend the procedures used in the pre-peak regime and to convert the load–deflection curve at a structural level into a stress–strain curve at a local level. However, in doing so, it is tacitly assumed that all hypotheses which are normally made to arrive at a continuum model and which have proven to be reasonable assumptions in the pre-peak regime still hold beyond peak stress level. One of these assumptions is that the transmission of forces between the material on both sides of an infinitesimal surface element is completely described by a force vector and does not require the introduction of a couple vector [1]. Rotational equilibrium of an elementary cube of material shows that this assumption is tantamount to the postulate that the stress tensor is

---

Correspondence to: Professor René de Borst, Delft University of Technology, Department of Civil Engineering/ TNO Building and Construction Research, P.O. Box 5048, 2600 GA Delft, The Netherlands.

symmetric, which is sometimes referred to as Boltzmann's Axiom. Nevertheless, continuum theories do exist that are not rooted in this assumption. Although such theories are usually much more complicated than classical continuum theories, their use is justified if the classical concept of a continuum fails to produce meaningful answers.

The transformation of an experimentally obtained load–displacement curve that exhibits a descending branch at the structural level into an affine stress–strain curve at the material point level is usually associated with the terminology 'strain-softening'. A constitutive law which has a descending branch in the stress–strain curve is then named a strain-softening type constitutive law.

In the last few years, the notion has transpired that a straightforward translation of load–displacement curves into stress–strain curves entails some serious complications, both from a mathematical and a physical point of view [2–5]. From a mathematical viewpoint, which will be the prime subject of concern in this contribution, we face the problem that introduction of strain softening in a classical continuum model may convert the boundary value problem for static loading conditions from an elliptic problem into a hyperbolic problem. For dynamic loading conditions on the other hand, hyperbolicity is lost and the wave speeds of loading waves become imaginary. In both cases, the rate boundary value problem is no longer well-posed. Numerically, this ill-posedness manifests itself in pathological mesh dependence, i.e. localisations which inevitably accompany failure processes in the classes of materials discussed above tend to be determined entirely by the spacing of the finite element mesh in lieu of being governed by the physics of the underlying problem [6, 7].

For transient problems, the loss of hyperbolicity and the ensuing pathological mesh sensitivity can, at least partially, be remedied by the consideration of heat flow and the inclusion of thermo-mechanical coupling terms and/or by resorting to the introduction of viscosity in the constitutive description [8–12]. These approaches implicitly introduce an internal length scale into the governing set of equations, which causes the initial value problem to remain well-posed.

For static loading conditions, the above enhancements of the constitutive model apparently cannot introduce an internal length scale into the problem. In the past, three different approaches have been followed to introduce such an internal length scale. The first approach introduces higher-order strain gradients in the constitutive description [13–18], while the second method employs an averaging procedure with respect to the inelastic state variables (non-local constitutive equations [19, 20]). The approach pursued in this paper is the use of a so-called generalised or micro-polar continuum. Such a continuum model, in which three rotational degrees-of-freedom are introduced in addition to the conventional three translational degrees-of-freedom, was proposed as early as in 1909 by E. and F. Cosserat [21]. Probably because of its relative complexity, it received little attention. Nevertheless, renewed interest arose after a dormant period of some 50 years, primarily due to the works of Eringen [22], Günther [23], Mindlin [24, 25], Schaefer [26, 27] and Toupin [28]. These contributions have considerably broadened the original concept of E. and F. Cosserat [21] and the terminology *micro-polar elasticity* has become the vogue to describe these extended or generalised elasticity theories. Yet, interest died in the late 1960s, probably because of the inherent complexity of the theory, which results in a governing set of differential equations that is insoluble except for the most simple cases [24, 26]. Other arguments against the use of micro-polar elasticity were put forward by Koiter [1] who unfortunately based his conclusions on a rather special type of micro-polar elastic solid, which may have blurred a proper assessment.

Recent years have again witnessed a proliferation of interest in micro-polar solids, as evidenced in the contributions of Bogdanova-Bontcheva and Lippmann [29] and Mühlhaus and Vardoulakis [30–32, 37]. In these approaches the emphasis is on *micro-polar plasticity* rather than on elasticity and it has been stressed that micro-polar theories by their very nature introduce a characteristic length in the constitutive description, thus rendering the governing set of equations to remain elliptic while allowing for localisation of deformation in a narrow, but finite band of material. In this paper we shall amongst other things show that these favourable properties are preserved also after discretisation of the continuum into finite elements.

Before entering the discussion how to implement Cosserat elasto-plasticity in a finite element context, including aspects such as temporal integration of the constitutive equations and consistent linearisation of the so-derived return-mapping algorithm, a brief discussion of the scope, the merits and limitations of the approach pioneered here is in order. First, the prime motivation of the present investigation was to construct a model that does not suffer from pathological mesh dependence as encountered in conventional strain-softening models for soils, concrete and rock, while being straightforwardly extendible to two and three dimensions. This goal has been reached completely. A limitation of the developed micro-polar, pressure-dependent J_2-flow theory is that it cannot realistically model mode-I fracture which is the prominent failure mechanism in concrete and rock under low confining pressures. For the latter class of problems, the inclusion of higher-order gradients in the constitutive model appears to be more effective [13]. More work is also needed on additional experimentation and extraction of material properties from test data, an issue that is only marginally addressed in this investigation. For instance, in the examples at the end of the paper the characteristic length has been chosen rather arbitrarily.

2. Cosserat elasticity

In the present treatment, we limit our attention to two-dimensional, planar deformations. In that case, each material point in a micro-polar solid has two translational degrees-of-freedom, namely u_x and u_y and a rotational degree-of-freedom ω_z, the rotation axis of which is orthogonal to the x, y-plane. As in a standard continuum the normal strains are defined as

$$\varepsilon_{xx} = \frac{\partial u_x}{\partial x} \quad \text{and} \quad \varepsilon_{yy} = \frac{\partial u_y}{\partial y} \, . \tag{1a,b}$$

However, the shear strains are given a slightly modified form:

$$\varepsilon_{xy} = \frac{\partial u_x}{\partial y} + \omega_z \quad \text{and} \quad \varepsilon_{yx} = \frac{\partial u_y}{\partial x} - \omega_z \, . \tag{2a,b}$$

It is observed that only for the choice

$$\omega_z = \frac{1}{2} \left(\frac{\partial u_y}{\partial x} - \frac{\partial u_x}{\partial y} \right), \tag{3}$$

of the macro-rotation, do ε_{xy} and ε_{yx} become equal, thus maintaining symmetry of the strain tensor. This rather special case of micro-polar elasticity has been the subject of much research,

but has also given rise to some confusion. Mindlin [24] has constructed exact solutions for stress concentrations around circular holes for this theory, while Koiter [1], on the basis of this special theory, has concluded that, for plate flexure, micro-polar elasticity results in an increase in rigidity over that predicted by classical elasticity, that is unlikely to have 'remained unnoticed' had micro-polar elasticity effects been significant. Unfortunately, the impression is sometimes created that the theory originated by E. and F. Cosserat embodies assumption (3), which is not true, (cf. [22, 27, 28]). The original theory of E. and F. Cosserat does not require (3), although the possibility of constraining the theory by imposing (3) was noticed by them. Later, Eringen [22] named this special case of the Cosserat theory the 'indeterminate couple-stress theory'. In the remainder of this treatment, we will not use (3) and we will adhere to the original formulation of the Cosserats for deriving the elastic part of the theory.

In addition to normal strains and shear strains, Cosserat theory also requires the introduction of micro-curvatures

$$\kappa_{zx} = \frac{\partial \omega_z}{\partial x} \quad \text{and} \quad \kappa_{zy} = \frac{\partial \omega_z}{\partial y} . \tag{4a,b}$$

Anticipating the treatment for elasto-plasticity we will rather use the generalised curvatures $\kappa_{zx}l$ and $\kappa_{zy}l$, where l is a material parameter with the dimension of length. It is this parameter which effectively sets the internal length scale in the continuum, and therefore has the role of a 'characteristic length'.

The strain components introduced so far may be assembled in a vector,

$$\varepsilon = [\varepsilon_{xx}, \varepsilon_{yy}, \varepsilon_{zz}, \varepsilon_{xy}, \varepsilon_{yx}, \kappa_{zx}l, \kappa_{zy}l]^t . \tag{5}$$

Note that in addition to the strain components introduced in (1), (2) and (4), the normal strain in the z-direction, ε_{zz}, has also been included in the strain vector ε. This has been done because, although this strain component remains zero under plane strain conditions during the entire loading process, this is not necessarily the case for the elastic and plastic contributions of this strain component. Also, the normal stress σ_{zz}, which acts in the z-direction, may be non-zero, which necessitates inclusion of ε_{zz} and σ_{zz} in the stress–strain relation. It is furthermore noted that by multiplying the micro-curvatures κ_{zx} and κ_{zy} by the length parameter l, all components of the strain vector ε have the same dimension.

Let us now consider the statics of a Cosserat continuum. While the strain vector ε is comprised of seven components for planar deformations, so is the stress vector σ. As in a classical continuum, we have the normal stresses σ_{xx}, σ_{yy} and σ_{zz}, and the shear stresses σ_{xy}, σ_{yx} (Fig. 1). For the Cosserat continuum, we also have to introduce stress quantities that are conjugate to the curvatures κ_{zx} and κ_{zy}. Figure 1 shows that the couple-stresses m_{zx} and m_{zy} serve this purpose. We observe that for this continuum model, a couple vector acts on an elementary surface in addition to the familiar stress vector.

Dividing the couple-stresses by the length parameter l, we obtain a stress vector σ in which all the entries have the same dimension:

$$\sigma = [\sigma_{xx}, \sigma_{yy}, \sigma_{zz}, \sigma_{xy}, \sigma_{yx}, m_{zx}/l, m_{zy}/l]^t . \tag{6}$$

Leaving aside body forces and body couples for the sake of simplicity (see e.g. [33] for an
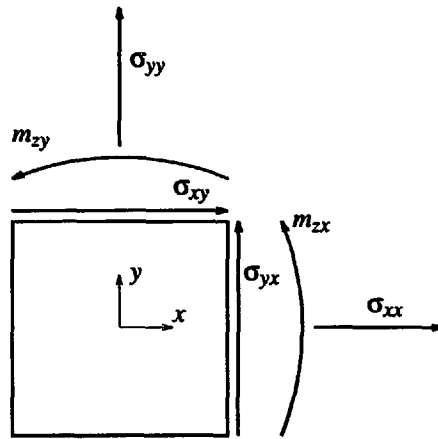
Fig. 1. Stress and couple-stress in a two-dimensional configuration.

extensive treatment), translational equilibrium in the x and y-directions results in

$$\frac{\partial \sigma_{xx}}{\partial x} + \frac{\partial \sigma_{xy}}{\partial y} = 0 , \qquad \frac{\partial \sigma_{yx}}{\partial x} + \frac{\partial \sigma_{yy}}{\partial y} = 0 , \tag{7a,b}$$

respectively, which replicates the result obtained for a classical, non-polar continuum. However, for rotational equilibrium, we find that

$$\frac{\partial m_{zx}}{\partial x} + \frac{\partial m_{zy}}{\partial y} - (\sigma_{xy} - \sigma_{yx}) = 0 , \tag{8}$$

which shows that the stress tensor is in general only symmetric ($\sigma_{xy} = \sigma_{yx}$) if the couple-stresses m_{zx} and m_{zy} vanish (Boltzmann's Axiom).

Anticipating the treatment of micro-polar plasticity in the next section, we decompose the strain vector into an elastic contribution $\boldsymbol{\varepsilon}^{e}$ and a plastic part $\boldsymbol{\varepsilon}^{p}$:

$$\boldsymbol{\varepsilon} = \boldsymbol{\varepsilon}^{e} + \boldsymbol{\varepsilon}^{p} , \tag{9}$$

while we assume that the elastic strain vector is linearly related to the stress vector $\boldsymbol{\sigma}$:

$$\boldsymbol{\sigma} = \boldsymbol{D}^{e} \boldsymbol{\varepsilon}^{e} ; \tag{10}$$

$\boldsymbol{D}^{e}$ is the stiffness matrix that contains the elastic moduli:

$$\boldsymbol{D}^{e} = \begin{bmatrix} 2\mu c_1 & 2\mu c_2 & 2\mu c_2 & 0 & 0 & 0 & 0 \\ 2\mu c_2 & 2\mu c_1 & 2\mu c_2 & 0 & 0 & 0 & 0 \\ 2\mu c_2 & 2\mu c_2 & 2\mu c_1 & 0 & 0 & 0 & 0 \\ 0 & 0 & 0 & \mu + \mu_c & \mu - \mu_c & 0 & 0 \\ 0 & 0 & 0 & \mu - \mu_c & \mu + \mu_c & 0 & 0 \\ 0 & 0 & 0 & 0 & 0 & 2\mu & 0 \\ 0 & 0 & 0 & 0 & 0 & 0 & 2\mu \end{bmatrix} , \tag{11}$$

with $c_1 = (1 - \nu)/(1 - 2\nu)$ and $c_2 = \nu/(1 - 2\nu)$. The elastic constants μ and ν have the classical meaning of the shear modulus and Poisson's ratio, respectively. μ_c is an additional material constant, completing the total of four material constants, viz. μ, ν, l and μ_c that are needed to describe the elastic behaviour of an isotropic Cosserat continuum under planar deformations. The coefficient 2 has been introduced in the terms D^e_{66} and D^e_{77} in order to arrive at a convenient form of the elasto-plastic constitutive equations. The total (bending) stiffness that sets the relation between the micro-curvatures and the couple-stresses is basically determined by the value of the internal length scale l.

We observe that all stiffness moduli that enter the elastic stress–strain matrix $\boldsymbol{D}^e$ have the same dimension. This is attributable to the fact that all components of the strain vector $\boldsymbol{\varepsilon}$ and the stress vector $\boldsymbol{\sigma}$ have the same dimension.

3. Micro-polar elasto-plasticity

In the present treatment, we employ a pressure-dependent J_2-flow theory (Drucker–Prager model). Accordingly, the yield function f can be written as

$$f = (3J_2)^{1/2} + \alpha p - \bar{\sigma}(\gamma) \,, \tag{12}$$

with $\bar{\sigma}$ a function of the hardening parameter γ and α a (constant) friction coefficient. $p = \frac{1}{3}(\sigma_{xx} + \sigma_{yy} + \sigma_{zz})$ and J_2 is the second invariant of the deviatoric stresses, which, for a micro-polar continuum, can be generalised as [30, 31]

$$J_2 = a_1 s_{ij} s_{ij} + a_2 s_{ij} s_{ji} + a_3 m_{ij} m_{ij}/l^2 \,. \tag{13}$$

In (13), the summation convention with respect to repeated indices has been adopted. s_{ij} is the deviatoric stress tensor and a_1, a_2 and a_3 are material parameters. In the absence of couple-stresses, i.e. $m_{ij} = 0$, $s_{ij} = s_{ji}$ and (13) reduces to

$$J_2 = (a_1 + a_2) s_{ij} s_{ij} \,, \tag{14}$$

which implies that the constraint $a_1 + a_2 = \frac{1}{2}$ must be enforced so that the classical expression for J_2 be retrieved properly.

For the case of planar deformations, J_2 can be elaborated as

$$J_2 = \frac{1}{2}[s_{xx}^2 + s_{yy}^2 + s_{zz}^2] + a_1\sigma_{xy}^2 + 2a_2\sigma_{xy}\sigma_{yx} + a_1\sigma_{yx}^2 + a_3[(m_{zx}/l)^2 + (m_{zy}/l)^2] \,. \tag{15}$$

Combining (12) and (15), and introducing the matrix

$$P = \begin{bmatrix} 2/3 & -1/3 & -1/3 & 0 & 0 & 0 & 0 \\ -1/3 & 2/3 & -1/3 & 0 & 0 & 0 & 0 \\ -1/3 & -1/3 & 2/3 & 0 & 0 & 0 & 0 \\ 0 & 0 & 0 & 2a_1 & 2a_2 & 0 & 0 \\ 0 & 0 & 0 & 2a_2 & 2a_1 & 0 & 0 \\ 0 & 0 & 0 & 0 & 0 & 2a_3 & 0 \\ 0 & 0 & 0 & 0 & 0 & 0 & 2a_3 \end{bmatrix} \tag{16}$$

then leads to an appealingly compact form of the yield function

$$f = [\tfrac{3}{2}\sigma^t P\sigma]^{1/2} + \alpha\sigma^t\pi - \bar{\sigma}(\gamma) , \tag{17}$$

with $\pi^t = [1/3, 1/3, 1/3, 0, 0, 0, 0]$. A (non-associated) flow rule is now obtained in an identical fashion to that in a non-polar continuum.

$$\dot{\varepsilon}^P = \dot{\lambda}\, \frac{\partial g}{\partial \sigma} , \tag{18}$$

where

$$g = [\tfrac{3}{2}\sigma^t P\sigma]^{1/2} + \beta\sigma^t\pi - \bar{\sigma}(\gamma) \tag{19}$$

is the plastic potential function and β is a dilatancy factor. Noting that during plastic flow $f = 0$, we obtain for the plastic strain rate

$$\dot{\varepsilon}^P = \dot{\lambda}\left[\frac{3P\sigma}{2\sqrt{3/2\sigma^t P\sigma}} + \beta\pi \right]. \tag{20}$$

In (18) and (20), $\dot{\lambda}$ is the plastic multiplier which, in analogy with classical plasticity, is determined from the consistency condition $\dot{f} = 0$.

It now remains to identify the plastic strain measure γ (the hardening parameter) for a J_2-flow theory in a Cosserat medium. For this purpose we first recall the conventional strain-hardening hypothesis,

$$\dot{\gamma} = [\tfrac{2}{3}\, \dot{e}_{ij}^P \dot{e}_{ij}^P]^{1/2} , \tag{21}$$

with $\dot{e}_{ij}^P$ the plastic deviatoric strain-rate tensor. For uniaxial stressing, $\dot{\gamma}$ reduces to the uniaxial plastic strain rate, $\dot{\gamma} = \dot{\varepsilon}_{xx}^P$. Since there are no couple-stress effects in uniaxial loading, we require that any modification to (21) for Cosserat media does not affect the result for pure uniaxial loading. Considering this prerequisite, a possible generalisation, analogous to (13), is to postulate that [30, 31]

$$\dot{\gamma} = [b_1 \dot{e}_{ij}^P \dot{e}_{ij}^P + b_2 \dot{e}_{ij}^P \dot{e}_{ji}^P + b_3 \dot{\kappa}_{ij}^P \dot{\kappa}_{ij}^P l^2]^{1/2} , \tag{22}$$

with $b_1 + b_2 = \tfrac{2}{3}$ in order that definition (21) for the strain-hardening hypothesis in a non-polar solid can be retrieved.

For the case of planar deformations, $\dot{\gamma}$ can be elaborated as

$$\dot{\gamma} = \left[\tfrac{2}{3}[(\dot{e}_{xx}^P)^2 + (\dot{e}_{yy}^P)^2 + (\dot{e}_{zz}^P)^2] + b_1(\dot{e}_{xy}^P)^2 + 2b_2 \dot{e}_{xy}^P \dot{e}_{yx}^P + b_1(\dot{e}_{yx}^P)^2 \right.$$
$$\left. + b_3[(\dot{\kappa}_{xz}^P l)^2 + (\dot{\kappa}_{yz}^P l)^2]] \right]^{1/2} . \tag{23}$$

Introduction of the matrix

$$Q = \begin{bmatrix} 2/3 & -1/3 & -1/3 & 0 & 0 & 0 & 0 \\ -1/3 & 2/3 & -1/3 & 0 & 0 & 0 & 0 \\ -1/3 & -1/3 & 2/3 & 0 & 0 & 0 & 0 \\ 0 & 0 & 0 & 3/2b_1 & 3/2b_2 & 0 & 0 \\ 0 & 0 & 0 & 3/2b_2 & 3/2b_1 & 0 & 0 \\ 0 & 0 & 0 & 0 & 0 & 3/2b_3 & 0 \\ 0 & 0 & 0 & 0 & 0 & 0 & 3/2b_3 \end{bmatrix} \tag{24}$$

allows the rate of the hardening parameter $\dot{\gamma}$ to be written in a similar format as the yield function,

$$\dot{\gamma} = \left[\tfrac{2}{3} (\dot{\varepsilon}^{\mathrm{P}})^{\mathrm{t}} Q \dot{\varepsilon}^{\mathrm{P}}\right]^{1/2} , \tag{25}$$

with the vector $\dot{\varepsilon}^{\mathrm{P}}$ assembling the plastic strain-rate components.

We next introduce the flow rule (20) in expression (23) for the rate of the hardening parameter. Since $\dot{\lambda}$ and $\bar{\sigma}$ are always non-negative, the result is given by

$$\dot{\gamma} = \dot{\lambda} \left(\frac{\sigma^{\mathrm{t}} P Q P \sigma}{\sigma^{\mathrm{t}} P \sigma}\right)^{1/2} \tag{26}$$

since $Q\pi = 0$. If the parameters a_1, a_2, a_3 and b_1, b_2, b_3 are chosen such that

$$PQP = P , \tag{27}$$

(25) reduces to exactly the same format as obtained in standard J_2-flow theory:

$$\dot{\gamma} = \dot{\lambda} . \tag{28}$$

In the remainder of this paper, we assume that condition (27) is satisfied.

With the above definitions, J_2-flow theory can be carried over to a Cosserat medium in a straightforward and elegant fashion. Integration algorithms for this model which are based on the concept of return mapping are discussed in the next section.

4. A return-mapping algorithm

With the governing rate equations for the micro-polar elasto-plastic solid at hand, we can set out to develop an algorithm that determines the stress increment in a finite loading step. Here, a variety of algorithms exist, but we shall only consider two possible candidates, namely the Euler backward algorithm and a one-step return-mapping algorithm in which the gradient is evaluated at the trial stress state,

$$\sigma_{\mathrm{t}} = \sigma_0 + D^{\mathrm{e}} \Delta\varepsilon , \tag{29}$$

σ_0 being the stress at the beginning of the loading step. For the latter algorithm, it has been shown in [34] that, for certain classes of the material parameters, there exists a set of values a_1, a_2, a_3 and b_1, b_2, b_3, which ensures a return to the yield surface in a single iteration. These advantageous properties are obtained for $a_1 = a_2 = \tfrac{1}{4}$, $a_3 = \tfrac{1}{2}$, $b_1 = b_2 = \tfrac{1}{3}$, $b_3 = \tfrac{2}{3}$. This set of constants will henceforth be referred to as the 'standard' set.

When these conditions are not satisfied, an Euler backward algorithm as delineated below should be employed. In this algorithm, the total strain increment in a finite loading step $\Delta\varepsilon$ is decomposed into an elastic contribution $\Delta\varepsilon^{\mathrm{e}}$ and a plastic part $\Delta\varepsilon^{\mathrm{P}}$,

$$\Delta\varepsilon = \Delta\varepsilon^{\mathrm{e}} + \Delta\varepsilon^{\mathrm{P}} . \tag{30}$$

Between the stress increment $\Delta\sigma$ and the elastic strain increment $\Delta\varepsilon^e$, we have the bijective relationship

$$\Delta\sigma = D^e\,\Delta\varepsilon^e\ .\tag{31}$$

Furthermore, the expression for the plastic strain rate (20) is integrated using a single-point Euler backward rule. This results in

$$\Delta\varepsilon^p = \Delta\lambda\left[\frac{3P\sigma_n}{2\sqrt{\frac{3}{2}\sigma_n^t P\sigma_n}} + \beta\pi\right],\tag{32}$$

where the subscript n refers to the value at the end of the loading step. By definition σ_n is given by

$$\sigma_n = \sigma_0 + \Delta\sigma\ ,\tag{33}$$

so that combination of (29)–(33) results in

$$\sigma_n = \sigma_t - \Delta\lambda\left[\frac{3D^e P\sigma_n}{2\sqrt{\frac{3}{2}\sigma_n^t P\sigma_n}} + \beta D^e\pi\right].\tag{34}$$

We next use the condition that at the end of the loading step the yield condition must be satisfied: $f(\sigma_n, \gamma_n) = 0$. Then, (34) transforms into

$$\sigma_n = \sigma_t - \Delta\lambda\left[\frac{3D^e P\sigma_n}{2[\bar{\sigma}(\gamma_n) - \alpha\pi^t\sigma_n]} + \beta D^e\pi\right].\tag{35}$$

A complication now arises, since we wish to express σ_n as a function of σ_t and $\Delta\lambda$, while in (35) σ_n also occurs in the denominator of the second term on the right-hand side. Therefore, we express $\pi^t\sigma_n$ as a function of $\pi^t\sigma_t$ and $\Delta\lambda$ by premultiplying (35) by the projection vector π. This gives

$$\pi^t\sigma_n = \pi^t\sigma_t - \Delta\lambda\beta K\ ,\tag{36}$$

with $K = \pi^t D^e\pi$. In the case of isotropic elasticity, K is the bulk modulus. Substitution of this identity into (35) results in the desired formulation:

$$\sigma_n = A^{-1}[\sigma_t - \Delta\lambda\beta D^e\pi]\ ,\tag{37}$$

where

$$A = I + \frac{3\Delta\lambda D^e P}{2[\bar{\sigma}(\gamma_n) + \Delta\lambda\alpha\beta K - \alpha\pi^t\sigma_t]}\ .\tag{38}$$

Substitution in the yield condition $f(\sigma_n, \gamma_n) = 0$ then results in a non-linear equation in $\Delta\lambda$,

$$f(\Delta\lambda) = (\tfrac{3}{2}(\sigma_t - \Delta\lambda\beta D^e\pi)^t A^{-t} P A^{-1}(\sigma_t - \Delta\lambda\beta D^e\pi))^{1/2} + \alpha\pi^t A^{-1}(\sigma_t - \Delta\lambda\beta D^e\pi) - \bar{\sigma}$$

$$= 0 , \tag{39}$$

which is solved using a Regula–Falsi method. Normally, convergence is achieved within 4–5 iterations.

5. Consistent linearisation moduli

For the derivation of a properly linearised set of tangential moduli, we will restrict ourselves to the format of a pressure-dependent J_2 micro-polar plasticity theory that obeys the constraint (27). Differentiating (34) then yields

$$\dot{\sigma} = H\left[\dot{\varepsilon} - \dot{\lambda}\,\frac{\partial g}{\partial\sigma}\right], \tag{40}$$

where

$$\frac{\partial g}{\partial\sigma} = \sqrt{\frac{3}{2}}\,\frac{P\sigma}{\sqrt{\sigma^t P\sigma}} + \beta\pi \tag{41}$$

and

$$H^{-1} = [D^e]^{-1} + \Delta\lambda\sqrt{\frac{3}{2}}\,\frac{\sigma^t P\sigma P - P\sigma\sigma^t P}{\sqrt{\sigma^t P\sigma}} . \tag{42}$$

Since $f = f(\sigma, \gamma)$, the consistency condition $\dot{f} = 0$ can be elaborated as

$$\left(\frac{\partial f}{\partial\sigma}\right)^t \dot{\sigma} + \frac{\partial f}{\partial\gamma}\,\dot{\gamma} = 0 . \tag{43}$$

Introducing the hardening modulus

$$h(\gamma) = \frac{\partial\bar{\sigma}}{\partial\gamma} \tag{44}$$

and using the yield condition (12), we obtain

$$\left(\frac{\partial f}{\partial\sigma}\right)^t \dot{\sigma} - h\dot{\lambda} = 0 . \tag{45}$$

Equation (45) can be combined with (40) to give the explicit consistent tangential stiffness relation

$$\dot{\sigma} = \left[H - \frac{H\,\dfrac{\partial g}{\partial\sigma}\left(\dfrac{\partial f}{\partial\sigma}\right)^t H}{h + \left(\dfrac{\partial f}{\partial\sigma}\right)^t H\,\dfrac{\partial g}{\partial\sigma}}\right]\dot{\varepsilon} . \tag{46}$$

6. Examples: shear layer and biaxial test

The model discussed in the preceding section has been implemented in a 6-noded triangular plane strain element. This element has 18 degrees-of-freedom due to the fact that each node has three degrees-of-freedom, two translations and one rotation.

To illustrate the effectiveness of the Cosserat model in predicting physically realistic solutions for mode-II failure problems, the shear layer of Fig. 2 has been analysed. It is assumed that the shear layer is infinitely long in both the negative and the positive x-direction. The discretisation of the shear layer, which has a height $H = 100$ mm, is shown in Fig. 2 for the case of 20 elements.

Basically, the problem is one-dimensional and could also have been analysed using line elements. Use of two-dimensional elements requires that linear constraint equations are added to the set of algebraic equations which result after discretisation of the continuum. They have to be applied to the displacements in the x-direction as well as to the rotational degrees-of-freedom, since all displacements in the y-direction are prevented (isochoric motion). The bottom of the shear layer is fixed ($u_x = 0$, $u_y = 0$) and the upper boundary is subjected to a shear force σ_{xy} (per unit area), which has been controlled using a standard arc-length technique [6, 7, 35]. The additional boundary condition $\omega_z = 0$ has been enforced at the lower and upper boundaries.

The standard elastic moduli have been chosen as shear modulus $\mu = 4000$ MPa and Poisson's ratio $\nu = 0.25$. The initial yield strength has been taken equal to $\bar{\sigma} = 100$ MPa, with no friction or dilatancy ($\alpha = \beta = 0$), while a linear softening diagram has been used with a hardening (softening) modulus $h = -0.125 \, \mu$. For the Cosserat continuum the additional material constants $\mu_c = 2000$ MPa and $l = 12$ mm have been inserted. Firstly, the standard values for a_1, a_2, a_3 and b_1, b_2, b_3 have been utilised.

In contrast to a standard continuum, a homogeneous strain state is not obtained under pure shear loading for a Cosserat continuum, at least not with the essential boundary conditions listed above. Already in the elastic regime a boundary layer with a height that is proportional to l develops at the upper and lower parts of the shear layer. As a consequence the localisation develops smoothly and gradually in the middle of the shear layer without the need for introducing imperfections or for adding a part of the eigenvector to the homogeneous solution [6, 7, 36].

When the discretisation is refined to such an extent that more than one set of two triangular elements are placed over the localisation zone, the width of the numerically predicted localisation zone becomes constant (Fig. 3). Figure 4(a) shows also that the load–displacement curve converges to a physically realistic solution.
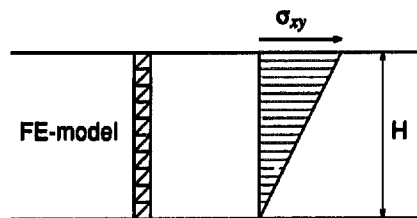

Fig. 2. Infinitely long shear layer: applied loading and finite element lay-out.
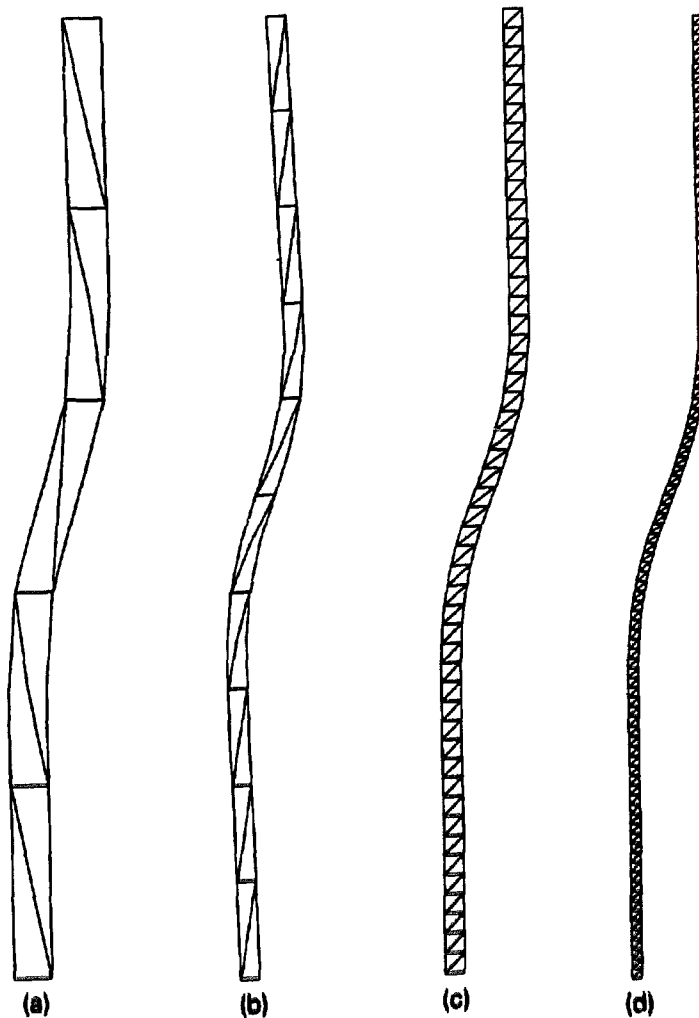
Fig. 3. Incremental displacement patterns at a residual load level of $\sigma_{xy}/\bar{\sigma} = 0.28$. (a) 10 elements; (b) 20 elements; (c) 100 elements; (d) 200 elements.

As alluded to in the introduction, a major question that needs to be addressed when introducing higher-order continuum models is the determination of the additional material parameters. The role of the internal length scale l is rather obvious, since it governs the brittleness and the width of the localisation zone. A smaller value for l implies a smaller width of the localisation zone and a steeper post-peak response as is shown in Fig. 4(b). The influence of the ratio $a_1 : a_2$ is shown in Fig. 4(c). Apart from the standard set ($a_1 = a_2 = \frac{1}{4}$), the so-called kinematic model of Mühlhaus and Vardoulakis [30, 31, 37] ($a_1 = \frac{3}{8}$, $a_2 = \frac{1}{8}$) and the static model of Mühlhaus and Vardoulakis [30, 31, 37] ($a_1 = \frac{3}{4}$, $a_2 = -\frac{1}{4}$) have been used. It appears that the specific choice of these parameters has little influence on the results in the first part of the post-peak regime, but that beyond some critical point in the post-peak regime, the gradual evolution of the localisation zone as observed for the standard model breaks down for the kinematic model and at an even earlier stage for the static model. Beyond these points, the kinematic and static models react in a very brittle manner. Finally, Fig. 4(d) shows the influence of the softening modulus on the structural behaviour.
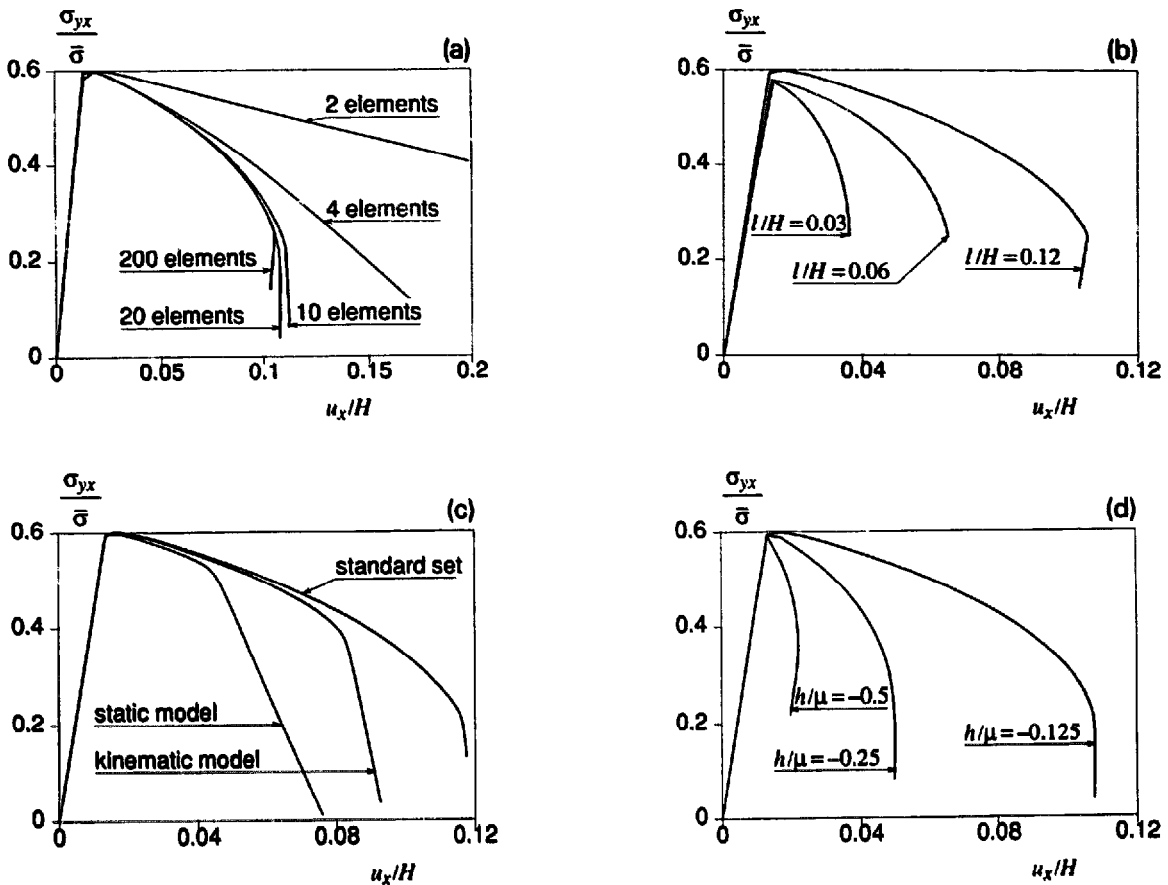
Fig. 4. Load–displacement diagram for shear layer. Results for a Cosserat continuum with strain softening. (a) The effect of mesh refinement; (b) the role of the characteristic length l; (c) influence of the parameter set (a_1, a_2, a_3); (d) influence of the softening modulus h.

To demonstrate the effectiveness of the Cosserat continuum also in two-dimensional boundary value problems where frictional sliding is the prevailing failure mechanism, a plane-strain biaxial test has been simulated. The specimen that has been considered has a width $B = 60$ mm and a height $H = 180$ mm. Smooth boundary conditions ($u_y = 0$) have been assumed at the upper and lower boundaries and natural boundary conditions have been
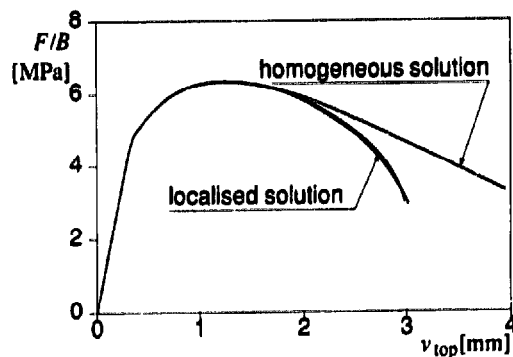

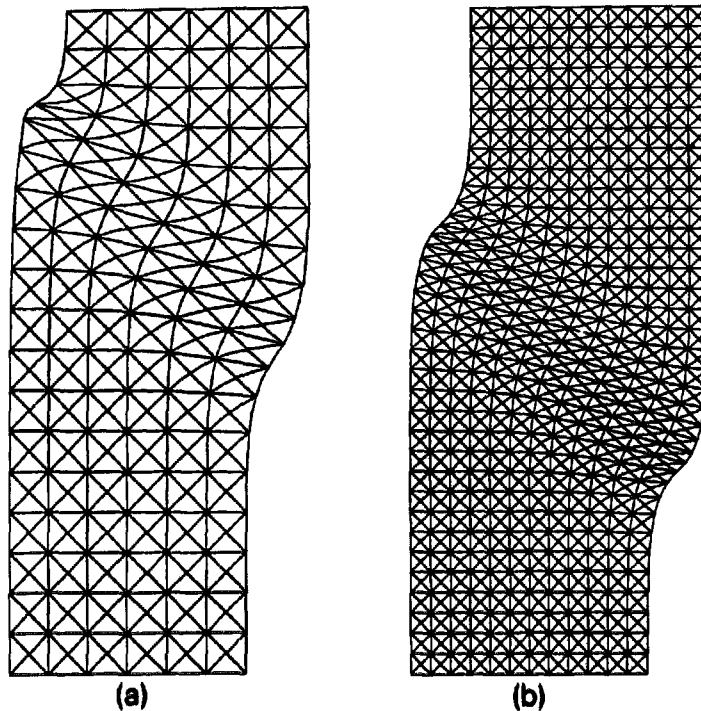Fig. 5. Load–displacement curves for a plane-strain biaxial test (Drucker–Prager yield function).

Fig. 6. Incremental displacements for a plane-strain biaxial test (Drucker–Prager plasticity). (a) Medium mesh with 432 elements; (b) Fine mesh with 1728 elements.

assumed at all sides for the rotations (ω_z free). A Drucker–Prager yield condition with a non-associated flow rule was employed. The material data were as follows: shear modulus $\mu = 1000$ MPa, Poisson's ratio $\nu = 0.2$, $\mu_c = 500$ MPa, $l = 6$ mm, $\alpha = 1.2$, $\beta = 0.0$ and $\bar{\sigma} = 1.2\sqrt{3}(1 - 25\gamma)$. For the coefficients a_1, a_2 and a_3 the 'standard' values have been analysed.

Three different meshes have been adopted, with 108, 432 and 1728 six-noded triangular elements, respectively. The load–displacement curves for all three discretisations are indistinguishable as is shown in Fig. 5. This figure also shows the solution that is obtained under the assumption of homogeneous deformations (no localisation).

Because in pure compression rotational degrees-of-freedom are not activated, an imperfect element (5% reduction in the initial yield strength) has been inserted in the model at the left boundary near the horizontal centre line. From this point, two shear bands initially propagate, but later only one band persists. The incremental displacements at this stage are shown in Fig. 6 for the medium (432 elements) and the fine mesh (1728 elements), respectively.

7. Concluding remarks

Micro-polar plasticity does not share the disadvantages that adhere to some other non-classical plasticity approaches. In particular, the concept of return-mapping algorithms can be applied straightforwardly and in a pointwise fashion. There is no need to restate the consistency condition in a format that involves distribution functions, as is the case for non-local approaches [38]. This observation greatly simplifies the programming effort.

Another important advantage is the fact that the major symmetry in the tangential stiffness matrix remains preserved when associated plasticity is used. Again, this result contrasts with non-local plasticity/damage theories with a local strain field, where this property is lost [19, 20].

Previous research on conventional strain-softening models [35, 39, 40] has shown that, when finite elements are used for such material models, the solution tends to become unstable at some stage of the loading process. Some elements or groups of elements tend to show deformation patterns that are totally unrealistic and physically unacceptable. The micro-polar approach, which basically enriches the element formulation with higher-order gradients, appears to stabilise the element behaviour when strain-softening type constitutive laws are used.

Acknowledgment

References

[1] W.T. Koiter, Couple-stresses in the theory of elasticity, I and II, Proc. Roy. Netherlands Acad. Sci. B67 (1964) 17–44.

[2] Z.P. Bazant, Instability, ductility and size effect in strain-softening concrete, ASCE J. Engrg. Mech. Div. 102 (1976) 331–344.

[3] H.E. Read and G.A. Hegemier, Strain softening of rock, soil and concrete – A review article, Mech. Mater. 3 (1984) 271–294.

[4] J.G. Rots and R. de Borst, Analysis of concrete fracture in 'direct' tension, Internat. J. Solids and Structures 25 (1989) 1381–1394.

[5] I.S. Sandler, Strain softening for static and dynamic problems, in: K.J. Willam, ed., Constitutive Equations: Macro and Computational Aspects (ASME, New York, 1984) 217–231.

[6] R. de Borst, Bifurcations in finite element models with a non-associated flow law, Internat. J. Numer. Anal. Methods Geomech. 12 (1988) 99–116.

[7] R. de Borst, Numerical methods for bifurcation analysis in geomechanics, Ing.-Arch. 59 (1989) 160–174.

[8] J. Lemonds and A. Needleman, Finite element analysis of shear localization in rate and temperature dependent solids, Mech. Mater. 5 (1986) 339–361.

[9] A. Needleman, Material rate dependence and mesh sensitivity in localization problems, Comput. Methods Appl. Mech. Engrg. 67 (1988) 69–85.

[10] T.G. Shawki and R.J. Clifton, Shear-band formation in thermal viscoplastic materials, Mech. Mater. 8 (1989) 13–43.

[11] L.J. Sluys and R. de Borst, Wave propagation and localisation in a rate-dependent crack medium: Model formulation and one-dimensional examples, Internat. J. Solids and Structures 29 (1992) 2945–2958.

[12] P. Wriggers, C. Miehe, M. Kleiber and J.C. Simo, On the coupled thermo-mechanical treatment of necking problems via finite element methods, Internat. J. Numer. Methods Engrg. 33 (1992) 869–884.

[13] R. de Borst and H.-B. Mühlhaus, Gradient-dependent plasticity: Formulation and algorithmic aspects, Internat. J. Numer. Methods Engrg. 35 (1992) 521–539.

[14] B.D. Coleman and M.L. Hodgdon, On shear bands in ductile materials, Arch. Rational Mech. Anal. 90 (1985) 219–247.

[15] D. Lasry and T. Belytschko, Localization limiters in transient problems, Internat. J. Solids and Structures 24 (1988) 581–597.

[16] H.-B. Mühlhaus and E.C. Aifantis, A variational principle for gradient plasticity, Internat. J. Solids and Structures 28 (1991) 845–858.

[17] H.L. Schreyer and Z. Chen, One-dimensional softening with localization, J. Appl. Mech. 53 (1986) 791–979.

[18] N. Triantafyllidis and E.C. Aifantis, A gradient approach to localization of deformation: I. Hyperelastic materials, J. Elasticity 16 (1986) 225–237.

[19] Z.P. Bazant and G. Pijaudier-Cabot, Nonlocal continuum damage, localization instability and convergence, ASME J. Appl. Mech. 55 (1988) 287–293.

[20] G. Pijaudier-Cabot and Z.P. Bazant, Nonlocal damage theory, ASCE J. Engrg. Mech. 113 (1987) 1512–1533.

[21] E. Cosserat and F. Cosserat, Théorie des Corps Deformables (Herman et fils, Paris, 1909).

[22] A.C. Eringen, Theory of micropolar elasticity, in: H. Leibowitz, ed., Fracture, An Advanced Treatise (Academic Press, New York, 1968) 621–729.

[23] W. Günther, Zur Statik und Kinematik des Cosseratschen Kontinuums, Abh. Braunschweig. Wiss. Ges. 10 (1958) 195–213.

[24] R.D. Mindlin, Influence of couple-stress on stress concentrations, Exp. Mech. 3 (1963) 1–7.

[25] R.D. Mindlin, Microstructure in linear elasticity, Arch. Rational Mech. Anal. 16 (1964) 51–78.

[26] H. Schaefer, Versuch einer Elastizitätstheorie des zweidimensionalen ebenen Cosserat-Kontinuums, in: M. Schaefer, ed., Miszellaneen der Angewandten Mechanik (Akademie Verlag, Berlin, 1962) 277–292.

[27] H. Schaefer, Das Cosserat-Kontinuum, Z. Angew. Math. Mech. 47 (1967) 485–498.

[28] R. Toupin, Elastic materials with couple-stresses, Arch. Rational Mech. Anal. 11 (1962) 385–414.

[29] N. Bogdanova-Bontcheva and H. Lippmann, Rotationssymmetrisches Fließen eines granularen Modellmaterials, Acta Mech. 21 (1975) 93–113.

[30] H.-B. Mühlhaus, Lamination phenomena in prestressed rock, in: Preprints 2nd Internat. Symp. on Rockbursts and Seismicity in Mines (University of Minnesota, Minneapolis, 1988) 117–128.

[31] H.-B. Mühlhaus and I. Vardoulakis, The thickness of shear bands in granular materials, Geotechnique 37 (1987) 271–283.

[32] H.-B. Mühlhaus, Application of Cosserat theory in numerical solutions of limit load problems, Ing.-Arch. 59 (1989) 124–137.

[33] C. Truesdell and W. Noll, The non-linear field theories of mechanics, The Encyclopedia of Physics, Vol. III/3 (Springer, Berlin, 1965).

[34] R. de Borst, Simulation of strain localization: A reappraisal of the Cosserat continuum, Engrg. Comput. 8 (1991) 317–332.

[35] M.A. Crisfield, Snap-through and snap-back response in concrete structures and the dangers of underintegration, Internat. J. Numer. Methods Engrg. 22 (1986) 751–768.

[36] R. de Borst, Non-linear analysis of frictional materials, Dissertation, Delft University of Technology, Delft, 1986.

[37] I. Vardoulakis, Shear-banding and liquefaction in granular materials on the basis of a Cosserat continuum theory, Ing.-Arch. 59 (1989) 106–113.

[38] J.C. Simo, Strain softening and dissipation: A unification of approaches, in: J. Mazars and Z.P. Bazant, eds., Cracking and Damage: Strain Localization and Size Effect (Elsevier, London, 1989) 440–461.

[39] R. de Borst, Analysis of spurious kinematic modes in finite element analysis of strain-softening materials, in: J. Mazars and Z.P. Bazant, eds., Cracking and Damage: Strain Localization and Size Effect (Elsevier, London, 1989) 335–348.

[40] J.G. Rots and R. de Borst, Analysis of mixed-mode fracture in concrete, ASCE J. Engrg. Mech. 113 (1987) 1739–1758.